Tightly coupled GPS/INS integration based on GPS carrier phase velocity update

S. Moafipoor [1,2], D.A. Grejner-Brzezinska [2], C.K. Toth [1]
[1] Center for Mapping, The Ohio State University
[2] Geodetic and Geoinformation Science, The Ohio State University

BIOGRAPHY

Mr. Shahram Moafipoor is currently a PhD student in the Department of Geodetic Science, The Tehran University, and a visiting scholar in the Department of Civil and Environmental Engineering and Geodetic Science, The Ohio State University. Prior to that, he was a researcher at National Cartography Center (NCC), Iran. He obtained an MS degree in photogrammetry from Tehran University in Tehran, Iran in 1998 and B.Sc in surveying from Tehran University in Tehran, Iran in 1993. His research interests include navigation systems, aerial photography, and digital photogrammetry.

Dr. Dorota Brzezinska is an Associate Professor in Geodetic and Geoinformation Science, The Ohio State University (OSU). Prior to that, she was a Research Specialist at the OSU Center for Mapping. She received an MS in Surveying and Land Management from the Agricultural and Technical University of Olsztyn, Poland, and an MS and a Ph.D. in Geodesy from OSU. Her research interests cover precise kinematic positioning with GPS, precision orbit determination for GPS/LEO, GPS/INS integration, mobile mapping technology, and robust estimation techniques. Between 1990-1995 she was a Fulbright Fellow at OSU. She is the 2003-2005 Land Representative for the ION Council, chair of IAG Sub-Commission 4.1, *Multi-sensor Systems*, a co-chair of the IAG Study Group 4.1, *Pseudolite Applications in Positioning and Navigation*, and a chair of the Task Force 5.3.1, *Mobile Mapping Systems* of FIG WG 5.3.

Dr. Charles Toth is a Senior Research Scientist at the Ohio State University Center for Mapping. He received an MS in Electrical Engineering and a Ph.D. in Electrical Engineering and Geoinformation Sciences from the Technical University of Budapest, Hungary. His research expertise covers broad areas of 2D/3D signal processing, spatial information systems, high-resolution imaging, surface extraction, modeling, integrating and calibrating of multi-sensor systems, multi-sensor geospatial data acquisition systems, and mobile mapping technology. He is Co-Chairing ISPRS WG II/2 on LiDAR and InSAR Systems and serves as the Assistant Director for the Photogrammetric Application Division of ASPRS.

ABSTRACT

In the majority of multi-sensor mapping systems, the GPS/INS integration serves as a navigation and georegistration tool, supporting the simultaneously acquired imagery. In a tightly coupled integration architecture, where double difference (DD) GPS carrier phase observations and the IMU (inertial measurement unit) accelerometer and gyroscope data are integrated in a single centralized Kalman filter, any loss of GPS signal causes a discontinuity in the filter measurement update until the signal reacquisition and the integer ambiguity recovery. Long GPS gaps may cause IMU error growth, and thus, positioning error increase, which may prevent instantaneous ambiguity recovery, especially for longer baselines and noisy environments. If the time needed to fix the new ambiguities is excessive, preventing the filter from using any GPS information, it may be beneficial to switch to either triple differences (they do not require ambiguity fixing, as ambiguities are eliminated by the third difference), or to velocities derived from the carrier phase observations. Extracting the GPS velocity from the carrier phase observation, which is independent of the ambiguity value, offers an opportunity to calibrate the IMU sensors, and to maintain the high quality navigation parameter estimation.

This paper presents a filter update method based on GPS velocity calibration in the GPS/INS integration system, to assure availability and continuity of the navigation solution. The algorithm is implemented and validated based on the data obtained by the AIMS^{TM} system, originally developed at the Center for Mapping, The Ohio State University. AIMS^{TM} utilizes the DD GPS carrier phase observable as the measurement update (and requires integer ambiguity values), while the method presented here is based on introducing the GPS velocity derived from the carrier phase observable to bridge these portions of the trajectory, where GPS signal is partially or entirely available, but the integer ambiguities cannot be established. The preliminary results indicate that steady navigation accuracy can be maintained for the entire trajectory. Moreover, the GPS velocity information, combined with the DD carrier phase, is likely to improve the filter's sensitivity to the platform maneuvers.

1. INTRODUCTION

GPS/INS is the most frequently used integrated multi-sensor navigation and guidance system, while the GPS/INS/CCD camera combination is often used for precise mapping, where GPS/INS provide directly the Exterior Orientation Parameters (EOP) of the captured images. Since the INS sensors suffer from imperfection of accelerometers and gyroscopes, which cause integration (and thus, navigation) error growth with time, these sensors should be calibrated with some type of non-inertial observations, such as GPS, Distance Measurement Equipment (DME) and image data [1]. The integration of GPS/INS is done in the process called Kalman filtering. There are two primary integration modes loosely coupled and tightly coupled systems; tightly coupled based on centralized Kalman filter is preferred [2]. In tightly coupled integration all position error states and error parameters corresponding to both systems GPS and INS are estimated simultaneously within one Kalman filter; moreover the INS errors are fed back directly to the INS sensor [3]. In a tightly coupled integration architecture, where double difference (DD) GPS carrier phase observations and the IMU accelerometer and gyroscope data are integrated in a single centralized Kalman filter, any loss of GPS signal causes a discontinuity in the filter measurement update until the signal reacquisition and the integer ambiguity recovery. Meanwhile, a robust navigation system should be able to accommodate all unexpected events, and to preserve consistency of the navigation data. If the time needed to fix the new ambiguities is excessive, preventing the filter from using any GPS information, it may be beneficial to switch to velocities derived from the carrier phase observations or to triple differences. Even though the noise will be increased by additional differencing operation, the continuity of the solution may be preserved.

This paper suggests using a Kalman filter method based on GPS velocity, which is independent of the ambiguity terms (but subject to cycle slips), in order to maintain the continuity of the navigation solution. The algorithm is implemented and validated based on the data obtained by the AIMS^{TM} system, originally developed at the Center for Mapping, The Ohio State University [3].

AIMS^{TM} utilizes the DD GPS carrier phase observable as the measurement update (and requires integer ambiguity values), while the method presented here is based on introducing the GPS velocity derived from the carrier phase observable to bridge these parts of the trajectory, where GPS signal is partially or entirely available, but the integer ambiguities cannot be established. Furthermore, the combination of DD GPS carrier phase and GPS velocity offers an opportunity to improve the filter measurement update step.

Section 2 of this paper discusses the method used to extract the GPS velocity, and Section 3 explores the velocity filter design. The cycle slip detection strategy, compatible with the new filter, is the issue discussed in Section 3.1. The numerical tests are presented in Section 4. The filter measurement update optimization with the combination of DD GPS carrier phase and GPS velocity is tested in Section 5. Finally, summary and conclusions are presented.

2. LINE OF SIGHT GPS VELOCITY

The velocity vector can be extracted from the GPS measurements in two methods. The first option is using the Doppler raw measurement, which provides directly the radial velocity from Phase Lock Loop (PLL) [4], and the second method uses a basic form of the carrier phase measurements [5]. It is known that the phase velocity estimation is more accurate than Doppler observations [6]. The phase rate method is chosen in this paper to estimate the GPS velocity, although, the Doppler raw observations are also used later to detect the cycle slips.

The one-way carrier phase between receiver *A* and satellite *j* is given by:

$$\Phi_A^j(t) = \rho_A^j(t) - \frac{I_A^j(t)}{f_i^2} + T_A^j(t) + \lambda_i N_A^j(t) + c(dt_A - dt^j) + M_A^j(t) + \varepsilon_i \quad (1)$$

$$\rho_A^j = \left\| \vec{X}^j - \vec{X}_A \right\| = \vec{e}_A^j \vec{X}_A^j = \vec{e}_A^j (\vec{X}^j - \vec{X}_A) \quad (2)$$

where Φ_A^j is the observed difference between the phase transmitted by satellite *j* and the phase generated by receiver *A*, ρ_A^j is the geometric distance between satellite *j* at transmit time and receiver *A* at the receive time, I_A^j / f_i^2 is the ionospheric delay, T_A^j is the tropospheric delay, dt_A is the clock error of receiver *A*, dt^j is the clock error of satellite *j*, N_A^j is the integer number of cycles, M_A^j is the multi-path effect, ε_i is the remaining white noise, f_i is the nominal frequency of the carrier wave for L_1, L_2, respectively, where subscript *i = 1, 2*, and $\vec{e}_A^j$ is the line of sight unit vector in the direction of the vector $\vec{X}_A^j$.

Performing the first time derivative of the one-way phase in equation (1) provides the line of sight velocity in equation (3).

$$\dot{\Phi}_A^j(t) = \dot{\rho}_A^j(t) + c(d\dot{t}_A - d\dot{t}^j) + \dot{\varepsilon}_i \quad (3)$$

$$\dot{\Phi}_A^j \approx \frac{\Phi_A^j(t+\Delta t) - \Phi_A^j(t)}{\Delta t} \quad (4)$$

$$\dot{\rho}_A^j = \vec{e}_A^j \dot{\vec{X}}_A^j = \vec{e}_A^j (\dot{\vec{X}}^j - \dot{\vec{X}}_A) \quad (5)$$

where $\dot{\Phi}_A^j$ is the phase rate, $\dot{\rho}_A^j$ is the line of sight velocity between satellite j and station A, and $d\dot{t}^j$, $d\dot{t}_A$ are clock rate terms of the satellite and the receiver, respectively, and Δt is the GPS data rate, $\dot{\vec{X}}^j$ is the satellite velocity vector, and $\dot{\vec{X}}_A$ is the station velocity vector. It is clear that the first derivative of one-way phase eliminates the unknown integer number of cycles. It is also assumed here that the atmospheric delays are constant over the short time period, however any deviations from this assumption will be absorbed in the noise component $\dot{\varepsilon}_i$.

While the line of sight velocity corresponds to the scalar range rate term, $\dot{\rho}_A^j$, in geometric terms, two parameters of direction and magnitude are needed to express the velocity vector. The direction of the velocity vector is determined based on the unit vector, $\vec{e}_A^j$, at the prior rover position, and the vector length, $\left\|\dot{\vec{X}}_A\right\|$, is resolved based on satellite velocity, $\dot{\vec{X}}^j$, and the carrier phase rate $\dot{\Phi}_A^j$.

The DD carrier phase rate formula, for the base station *A*, and rover station *B*, is expressed in equation (6), which is independent of the clock bias and atmospheric terms.

$$\dot{\Phi}_{AB}^{jk} = (\vec{e}_B^k \dot{\vec{X}}_B^k - \vec{e}_B^j \dot{\vec{X}}_B^j) - (\vec{e}_A^k \dot{\vec{X}}_A^k - \vec{e}_A^j \dot{\vec{X}}_A^j) + \ddot{\varepsilon} \quad (6)$$

This equation includes the velocity vector of the rover station, $\dot{\vec{X}}_B$, which can be determined with at least three line of sight observations in either dual-frequency or single-frequency phase observations together with the velocity weight matrix, which is computed by applying the covariance propagation law to the relation of phase rate in equation (6).

In order to assess the algorithm, two different tests, static and kinematic, were performed. In the static mode, the RMS is computed based on the expected zero velocity of station. The RMS of N-E-H components of velocity vector were estimated as (0.7, 1.0, 1.1) mm/s. The kinematic test was provided with a flight over Tucson, Arizona, in May 2002, using the AIMS™ hardware. The effective baseline reached over 55 km. The kinematic test trajectory is shown in Figure 1.

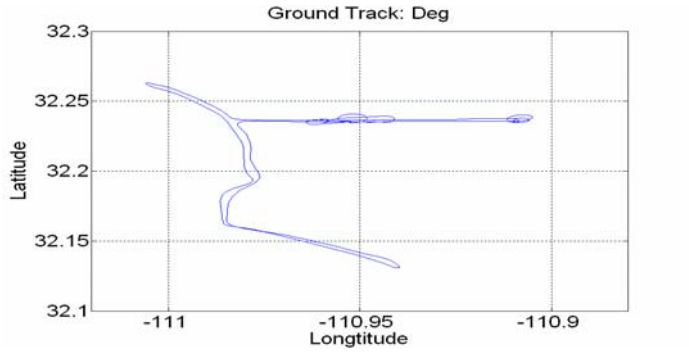

Figure 1: Kinematic test flight trajectory

The reference navigation parameters were calculated with the STD better than 3 cm for position and 2 mm/s for velocities, as well as 6 arcsec for attitudes, respectively. The differences between the known velocity vectors, computed by the DD carrier phase-based (reference) GPS/INS Kalman filter, and the carrier phase velocity components are plotted in Figure 2. The RMS of fit equal to (4.7, 5.8, 4.2) mm/s, in N-E-H directions, is determined for the data including high dynamic maneuvers (high dynamics is defined here according to [7] as acceleration >3 m/s^2 and jerk<0.5 m/s^3).

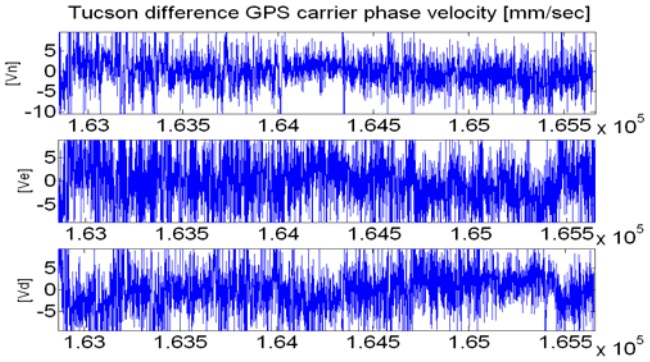

Figure 2: The GPS velocity difference in N-E-H between the reference velocity and velocity-based solution

3. VELOCITY FILTER DESIGN

The mobile mapping systems, in particular land-based systems often suffer from losses of GPS lock. In these cases, the navigation parameters are determined in the free inertial navigation mode. Consequently, due to the lack of external aiding, the inertial navigation system exhibits errors growing with time. These errors, in the

Schuler-tuned INS, tend to grow exponentially with time in the vertical channel, while the error in the horizontal channels tends to grow no faster than a sinusoidal pattern with linearly increasing envelope in [8]. To limit the error growth during the free navigation mode, the system should be supported by some external measurements, such as the static INS calibration in so-called Zero Velocity update (ZUPT) mode [9]. As an option, the proposed method discusses the calibration of an inertial system in dynamic mode, where the velocity provides the required information for the calibration process. To design the filter in a tightly coupled integration, the differential error model and observation model should be determined.

Various forms of INS error models have been developed, however, all these models can be derived using a unified approach, and considered equivalent. The INS error model used in here, is based on the psi-angle approach model developed by [10]:

$$\begin{aligned}
\delta\dot{r}^n &= -\omega_{en}^n \times \delta r^n + \delta v^n \\
\delta\dot{v}^n &= -\psi^n \times f^n + C_b^n \delta f^b - (2\omega_{ie}^n + \omega_{en}^n) \times \delta v^n \\
&\quad - (2\delta\omega_{ie}^n + \delta\omega_{en}^n) \times v^n + \delta g^n \\
\dot{\psi}^n &= \delta\omega_{in}^n - (\omega_{in}^n \times)\psi^n - C_b^n \delta\omega_{ib}^b
\end{aligned} \tag{7}$$

where $\delta r^n, \delta v^n, \psi^n$ are the position, velocity and attitude error vectors respectively projected in *n-frame*, C_b^n is direction cosine matrix from *b-frame* to *n-frame*, f^n is the accelerometer sensed specific force vector transferred to the *n-frame* by $f^n = C_b^n f^b$, δf^b is the accelerometer bias, ω_{in}^n is the rotation rate vector of the *n-frame* with respect to the *i-frame* projected to the *n-frame*, ω_{en}^n is the rotation rate vector of the *n-frame* with respect to the *e-frame*, ω_{ie}^n is the rotation rate vector of the *e-frame* with respect to the *i-frame*, δg^n is the gravity anomaly error, $(\theta\times)$ means a skew symmetric matrix of argument θ, ω_{ib}^b is the Gyro output, and $\delta\omega_{ib}^b$ s the Gyro drift error.

The observation model of the filter is based on two types of measurements. The first is the velocity observation determined by GPS phase rate, and the second is the heading, derived from GPS position vectors.
Since the major objective of GPS/INS integrated system is providing the navigation parameters, it is expected that the GPS velocity measurements should be able to meet this objective, under the assumption that the absolute location is known at the starting epoch. Naturally, the velocity observation cannot directly estimate the position error due to lack of observability. The system observability defines the ability of state-space model to determine the state from the measurements [11]. Converting the velocity observation to the position coordinates can be achieved using equation (8):

$$\vec{x}_{t+\Delta t} = \vec{x}_t + \vec{v}_t . \Delta t \tag{8}$$

where Δt is the data sampling rate. The second type of external observation is heading, computed based on two sequential GPS observations, which form a direction. As an option, heading can be computed from multiple GPS antennas (at least two).

The difference between heading angles observed with GPS and INS systems establishes the second observation model of the Kalman filtering, which is discussed later. To derive this observable, a two-step process is required. First, since the GPS coordinate system is in the earth fixed coordinate system, *e-frame*, while INS coordinate system is defined in the body frame, *b-frame*, a transformation is needed to transform the INS heading in *b-frame* to *e-frame*. Second, the INS system is typically running at higher rate than GPS does, and consequently, the averaging the INS heading over the GPS rate, Δt, should be performed according to:

$$\alpha_{INS} = \frac{1}{\Delta t} \int_0^{\Delta t} \alpha_j^{INS} dt \tag{9}$$

Through the INS alignment, the INS body frame, *b-frame*, is orientated with respect to north direction so as to measure the attitude in navigation frame *n-frame*. To account for a tilt, it is required to compensate the roll and pitch rotations. Since the north direction of both the *n-frame* and the *e-frame* are the same, it is not needed to transfer the heading observed in the *n-frame* to the *e-frame*. To obtain correct heading in the *e-frame*, the observed INS heading should be transformed according to equation (10):

$$\begin{bmatrix} Roll \\ Pitch \\ Heading \end{bmatrix}_n = R_{-roll} . R_{-pitch} \begin{bmatrix} Roll \\ Pitch \\ Heading \end{bmatrix}_b \tag{10}$$

The differential and observation equations needed to establish the filter are now completed. The state-space model defining the equations is expressed as:

$$\begin{aligned}
\dot{x} &= Fx + W \\
y &= Hx + V
\end{aligned} \tag{11}$$

where, x is the system state vector, y is observation vector, W is random forcing function, V is the observation residual, F is the system dynamic matrix and H is the design matrix.

If DD carrier phase are used, an optimal 18-state centralized Kalman filter, equation (12), estimates the errors of position, δr, velocity, δv, attitude, ψ, as well as errors in the inertial sensor such as accelerometer error vector, gyroscope drift error and gravity anomaly vector. The dynamic matrix *F* is represented as:

$$x^T = [\delta r^n \quad \delta v^n \quad \psi^n \quad x^n_{Acc} \quad x^n_{Gyro} \quad x_{Grav}] \quad (12)$$

$$F = \begin{bmatrix} (-\omega^n_{en}\times) & I & 0 & 0 & 0 & 0 \\ F_{vr} & F_{vv} & (f^n\times) & C^n_b & 0 & I \\ 0 & 0 & -(\omega^n_{in}\times) & 0 & -C^n_b & 0 \\ 0 & 0 & 0 & 0 & 0 & 0 \\ 0 & 0 & 0 & 0 & 0 & 0 \\ 0 & 0 & 0 & 0 & 0 & F_{gg} \end{bmatrix} \quad (13)$$

where the sub-matrices are expressed as:

$$F_{vr} = \begin{bmatrix} -g/R_e & 0 & 0 \\ 0 & -g/R_e & 0 \\ 0 & 0 & 2g/R_e \end{bmatrix}$$

$$F_{vv} = \begin{bmatrix} 0 & -(2\omega^n_{ie}+\dot{\lambda})\sin\varphi & \dot{\varphi} \\ (2\omega^n_{ie}+\dot{\lambda})\sin\varphi & 0 & (2\omega^n_{ie}+\dot{\lambda})\cos\varphi \\ -\dot{\varphi} & -(2\omega^n_{ie}+\dot{\lambda})\cos\varphi & 0 \end{bmatrix}$$

$$F_{\psi v} = \begin{bmatrix} 0 & -(\omega^n_{ie}+\dot{\lambda})\sin\varphi & \dot{\varphi} \\ (\omega^n_{ie}+\dot{\lambda})\sin\varphi & 0 & -(\omega^n_{ie}+\dot{\lambda})\sin\varphi \\ -\dot{\varphi} & (\omega^n_{ie}+\dot{\lambda})\sin\varphi & 0 \end{bmatrix}$$

$$F_{gg} = diag\begin{bmatrix} -\tau^g_N & -\tau^g_E & -\tau^g_D \end{bmatrix}$$

where R_e equals the Earth radius plus vehicle altitude, and τ^g is the time constant for the Markov process of gravity anomaly, and the *W* is all zero-mean Gaussian white noise vectors.

$$W^T = [w_r \quad w_v \quad w_\psi \quad w_{Acc} \quad w_{Gyro} \quad w_g] \quad (14)$$

When the velocity is used as measurement update, the δr vector cannot be directly observed, as already mentioned. However, equation (8) can be used to find the 3D position coordinates.

Going back to equations (6), the observation equations of GPS phase velocity and averaged heading (from, for example, multiple GPS antennas), can be presented as follows:

$$y = \begin{bmatrix} \dot{\rho}^{jk\ GPS}_{AB} & -\dot{\rho}^{jk\ INS}_{AB} \\ Az^{GPS} & -Az^{INS} \end{bmatrix} \quad (15)$$

$$= \begin{bmatrix} \dot{\Phi}^{jk}_{AB} - \left(\vec{e}^{\,k}_B \dot{\vec{X}}^{\,k}_B - \vec{e}^{\,j}_B \dot{\vec{X}}^{\,j}_B - (\vec{e}^{\,k}_A \dot{\vec{X}}^{\,k}_A - \vec{e}^{\,j}_A \dot{\vec{X}}^{\,j}_A)\right) \\ Az^{GPS} - Az^{INS} \end{bmatrix}$$

After linearization, the observation matrix is determined as:

$$y = Hx + V = \begin{bmatrix} H_{3*3} & 0_{3*12} & -\Omega^b_{nb} H_{3*3} \\ 0_{3*3} & I_{1*1} & 0_{3*14} \end{bmatrix} x + V \quad (16)$$

where, *I* is the unit matrix, *O* is zero matrix, and Ω^b_{nb} is the gyro-sensed platform rotation rate vector, and the observation sub-matrix is expressed as:

$$H_{3*3} = \begin{bmatrix} \dfrac{\partial \dot{\rho}^{jk\,INS}_{AB}}{\partial v_n} & \dfrac{\partial \dot{\rho}^{jk\,INS}_{AB}}{\partial v_e} & \dfrac{\partial \dot{\rho}^{jk\,INS}_{AB}}{\partial v_d} \end{bmatrix}^T \quad (16a)$$

where $\dot{\rho}^{jk\,INS}_{AB}$ is the line of sight velocity derived based on the INS velocity of rover station, $\dot{\vec{X}}^{\,INS}_B$, as:

$$\dot{\rho}^{jk\,INS}_{AB} = \vec{e}^{\,k}_B(\dot{\vec{X}}^{\,k} - \dot{\vec{X}}^{\,INS}_B) - \vec{e}^{\,j}_B(\dot{\vec{X}}^{\,j} - \dot{\vec{X}}^{\,INS}_B) - \vec{e}^{\,k}_A \dot{\vec{X}}^{\,k} + \vec{e}^{\,j}_A \dot{\vec{X}}^{\,j} \quad (17)$$

It should be mentioned that the INS velocity vector, $\dot{\vec{X}}^{\,INS}_B$, which is used in equation (17), should be transformed to the GPS phase center according to equation (18):

$$\begin{aligned} \vec{X}^{\,GPS}_B &= \vec{X}^{\,INS}_B + C^n_b \Delta\vec{r}^{\,b} \\ \dot{\vec{X}}^{\,GPS}_B &= \dot{\vec{X}}^{\,INS}_B + \dot{C}^n_b \Delta\vec{r}^{\,b}, \qquad \dot{C}^n_b = C^n_b \Omega^b_{nb} \end{aligned} \quad (18)$$

where Ω^b_{nb} is the rotation rate matrix of the *b-frame* with respect to the *n-frame* projected to the *b-frame*, and C^n_b is explained earlier at equation (7), and $\Delta\vec{r}_b$ is the lever arm vector.

3.1 CYCLE SLIP DETECTION

The evaluation of GPS velocity, equation (6), assumes the constant ambiguity; however, cycle slips may occur at any time. So, it is necessary to incorporate an algorithm to detect the cycle slips. To detect the cycle slip during the velocity update filter, the algorithm developed by Kim and Langly [12] is used here. The geometry free combination of phase rate in equation (19) contains three main terms. The first one is the ionosphere rate term; next is the clock bias rate terms and final one is, the ambiguity rate terms. Since the ionosphere rate delay and clock bias rate terms are sufficiently small to be ignored, the main cause of geometry-free difference is considered a cycle slip (20).

$$\dot{\Phi}^{jk}_{AB,f_1} - \dot{\Phi}^{jk}_{AB,f_2} = q\frac{\dot{I}^{jk}_{AB}}{f_1^2} + \Delta\dot{t}^{jk}_{AB,f_1} - \Delta\dot{t}^{jk}_{AB,f_2} + \lambda_1\dot{N}^{jk}_{AB,f_1}(t) - \lambda_2\dot{N}^{jk}_{AB,f_2}(t) \quad (19)$$

$$\dot{\Phi}^{jk}_{AB,f_1} - \dot{\Phi}^{jk}_{AB,f_2} = \lambda_1\dot{N}^{jk}_{AB,f_1}(t) - \lambda_2\dot{N}^{jk}_{AB,f_2}(t) \quad (20)$$

where q is a constant factor.

A cycle slip can be detected based on the comparison between the geometry-free combination of the phase rate in equation (20), with the geometry-free combination of the double difference phase rate in equation (21) which has established the threshold needed to detect a cycle slip:

$$\dot{\Phi}^{jk}_{AB,f_1} - \dot{\Phi}^{jk}_{AB,f_2} = D^{jk}_{AB,f_1} - D^{jk}_{AB,f_2} \quad (21)$$

where $E[\dot{\Phi}_{GF}] > k.\mathrm{cov}(D_{GF})$, and k is empirically selected factor. Any geometry-free combination of phase rate greater than the geometry free combination of Doppler observations ($D^{jk}_{AB,f_1}, D^{jk}_{AB,f_2}$) is suspected to have a cycle slip.

4. NUMERICAL RESULTS

The integrated GPS/INS system used in this study comprises two GPS dual-frequency Trimble receivers collecting data at 1 Hz rate, and an LN100 INS based on Zer0-lock Laser Gyro and A-4 accelerometer triad (0.8 nmi/h CEP, Gyro bias $0.003\circ$/h, and accelerometer bias $25\mu g$). The LN100 firmware, modified for AIMS^{TM} project, allows for access to the raw IMU data, updated at 256 Hz. The airborne data presented here are collected in May 2002 over Tucson Arizona.

To check the proposed filter, random 60-second intervals were selected throughout the data set to be processed with the velocity-updated filter that replaces the DD carrier phase for the selected periods of time. Figures 3-5 show the difference of position, velocity and heading angle with respect to the reference solution obtained from the reference filter (i.e. full DD-based solution), and Table 1 presents the statistical analysis of the navigation solution during the selected time.

The average RMS of fit in the position, velocity and heading about 7 cm, 2 mm/s and 5 arcsec respectively were computed for the selected times. The two peaks that appear in Figure 3-4 are directly coupled to the times with the high dynamic maneuver of the platform, as shown in Figure 6 (epochs 163500-164060).

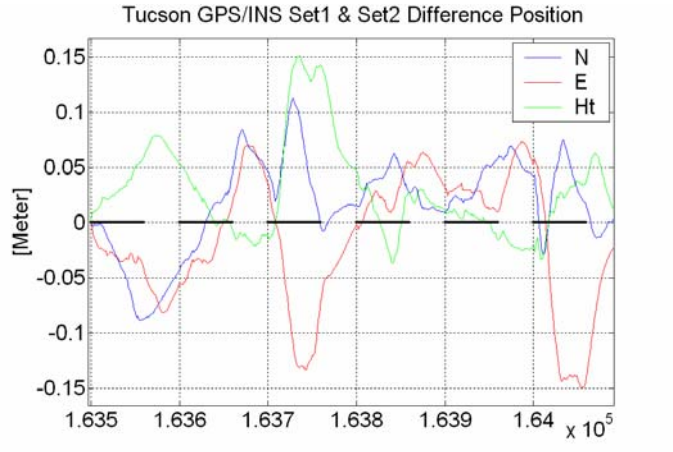

Figure 3: The position difference between the velocity-updated filter and the reference filter over selected time (60 sec) marked with the black lines

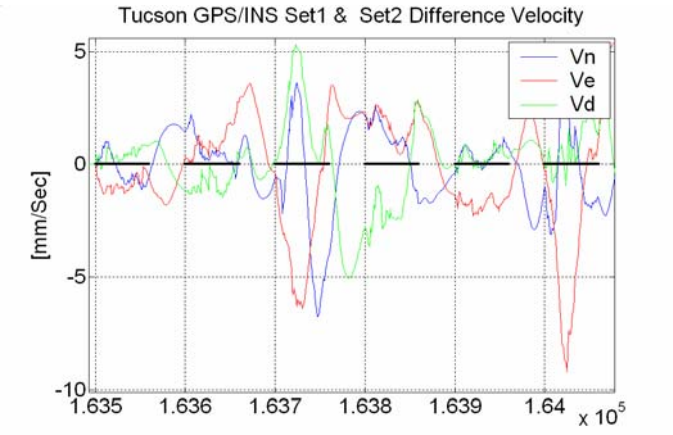

Figure 4: The velocity difference between the velocity-updated filter and the reference filter over selected time (60 sec) marked with the black lines

Filter Update period [sec]	Mean / STD	E	N	Ht	Mean / STD	v_n	v_e	v_d	Heading [Arcsec]
163500-163560	[m]	-0.038	-0.028	0.030	[mm/s]	-0.26	-0.86	0.43	0.37
	[cm]	3.1	0.7	1.4	[mm/s]	0.63	0.34	0.28	0.79
163600-163650		-0.002	-0.026	0.018		0.59	1.04	-0.79	-1.51
		2.4	2.0	1.8		0.65	0.68	0.49	2.03
163700-163760		0.057	-0.077	0.097		-1.5	-3.03	2.22	-0.77
		3.3	5.3	5.8		3.33	2.50	1.73	2.31
163800-163860		0.039	0.021	0.005		0.97	1.7	-0.13	1.84
		1.2	1.3	2.4		1.06	0.78	1.74	0.88
163900-163960		0.032	0.024	0.003		0.41	-1.7	0.29	4.82
		1.4	0.77	0.67		0.38	0.26	0.34	1.13
164000-164060		0.029	-0.085	0.013		-0.32	-3.23	0.80	17.31
		2.9	7.4	2.3		2.07	3.24	0.98	4.35

Table 1: The statistical analysis of the navigation parameters over selected time (60 sec)

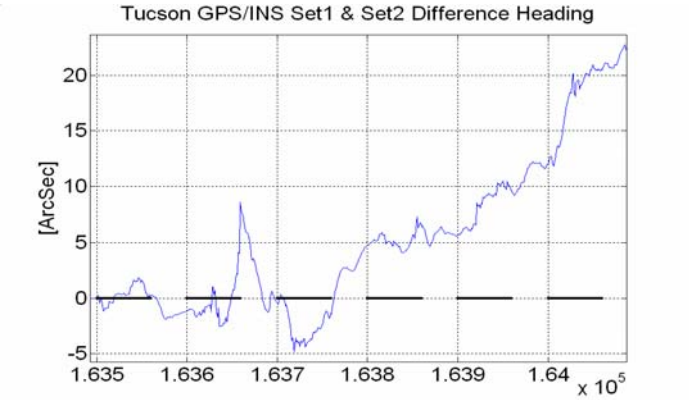

Figure 5: The heading difference between the velocity-updated filter and the reference filter over selected time (60 sec) marked with the black lines

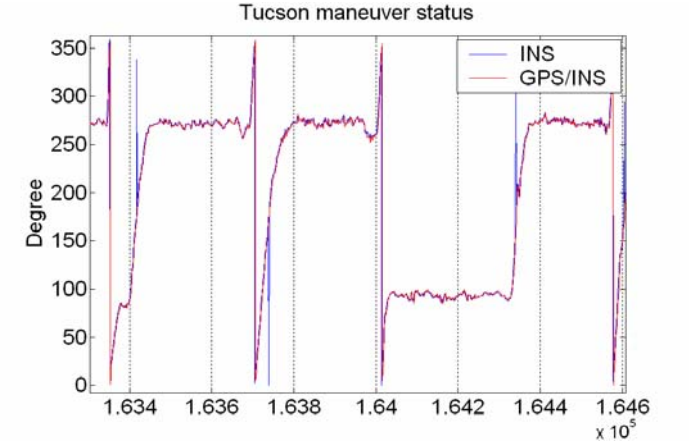

Figure 6: Heading over the selected time period

Based on the results presented in Table 1, it can be concluded that typically during the short time periods, the velocity-updated filter can provide the expected steady navigation accuracy, comparable to the DD-update filter, but mostly in low maneuver conditions; but in the high dynamic situation the results are different. This indicates that one of the solutions can capture the maneuvers much better.

In the second test, the velocity-updated filter was running over a larger time span of about 30 minutes. The selected data was also checked for the cycle slips with the method discussed in section 3.1. The differences of navigation parameters with respect to reference solution are shown in Figures 7-9.

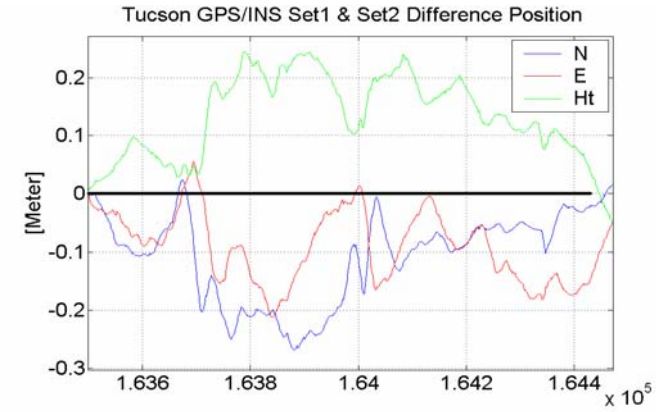

Figure7: The position difference of the velocity update filter

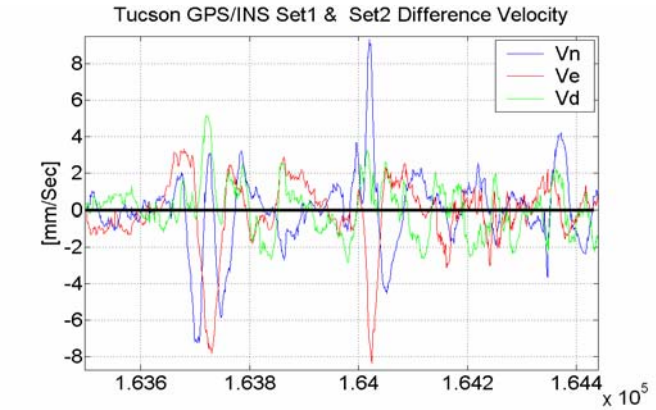

Figure 8: The velocity difference of the velocity update filter

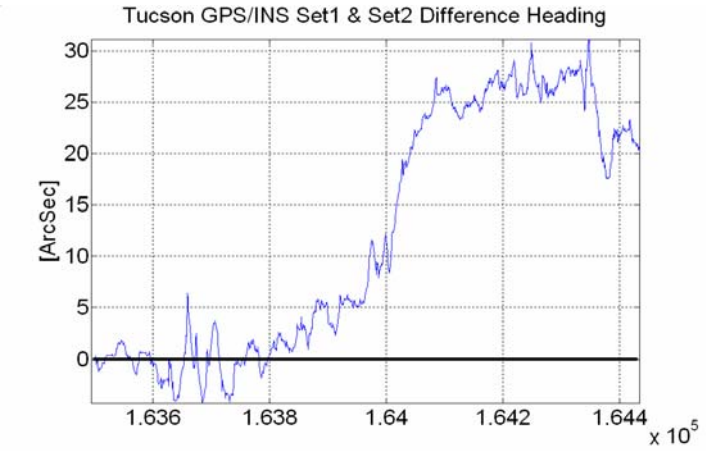

Figure 9: The heading difference of the velocity update filter

The average RMS of the position, velocity and heading angle about 14 cm, 3 mm/s and 20 arcsec, respectively, were derived based on the data (residuals plotted in Figurers 7-9) including sharp maneuvers, as shown in Figure 6 (epochs 163500-164420). Clearly, the maneuvers of the platform affected the quality of the navigation solution.

Figures 10-13 present the plot of the STD for the navigation parameters obtained with the velocity-updated filter, as compared with the reference filter. Clearly, the STD in horizontal positions indicates similar quality, but the vertical channel accuracy is improved. Similarly, the vertical velocity is improved more than the horizontal velocity components. The STD for heading angle between the two solutions remains the same.

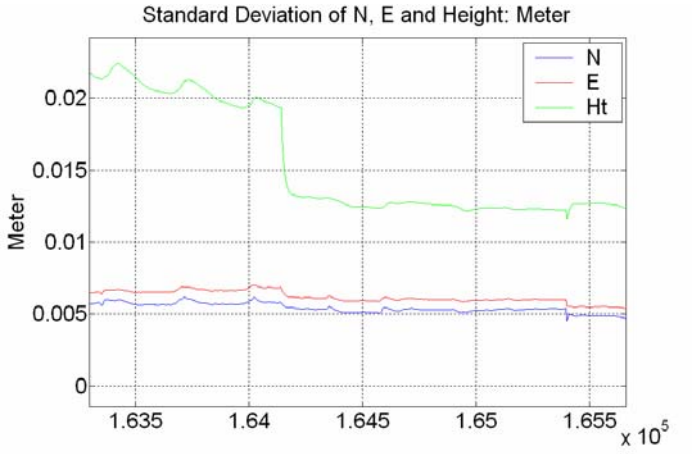

Figure 10: The STD of position in reference filter

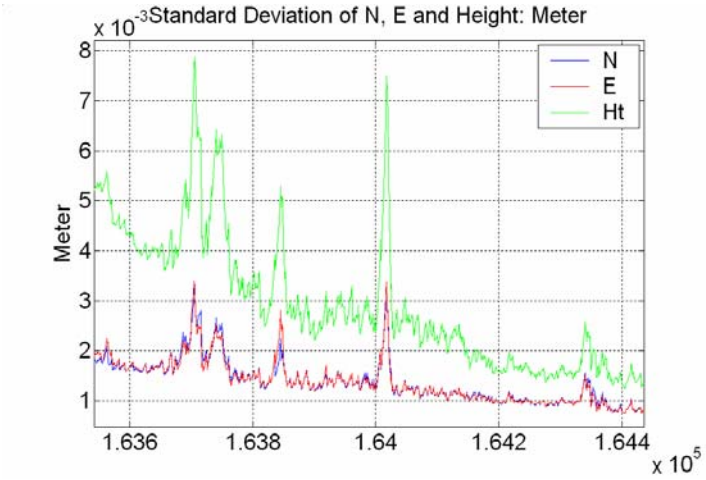

Figure 11: The STD of position in velocity-updated filter

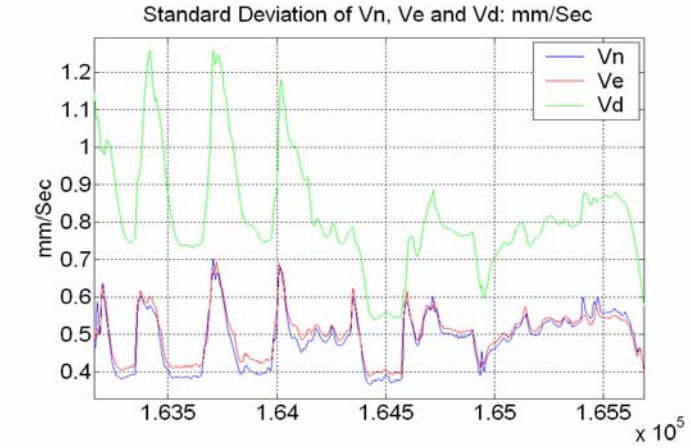

Figure 12: the STD of velocity in reference filter

Although the estimated STD of the navigation solutions is improved, the precision of theses parameters is still affected by the maneuvers. Moreover, the position error, which is derived based on the velocity measurement error, tends to accumulate with time, and could be corrected with IMU heading observations.

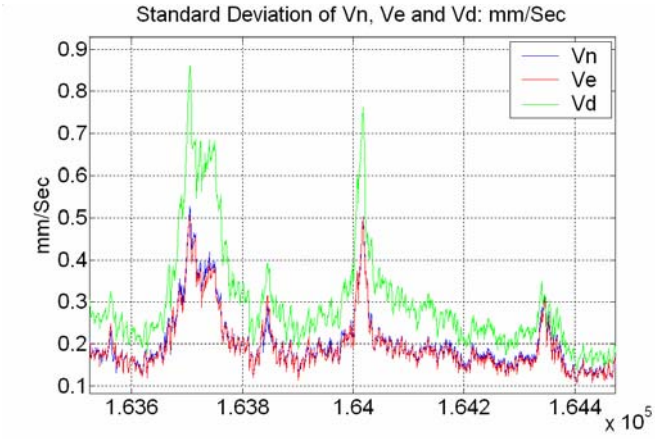

Figure 13: The STD of velocity in velocity-updated filter

5. EXTENDED MESUEMENT UPDATE FILTER

Kalman filter is not sensitive to the instant changes of state parameters [11]. In fact, most of the airborne mapping systems operate under high rate of change in velocity and heading conditions. The GPS velocity information, combined with the DD carrier phase, is likely to improve the filter's sensitivity to the platform maneuvers. In order to demonstrate the impact of the dynamic's of the platform, the extended measurement update step, based on position and velocity combinations was tested over the selected trajectory.

As a comparison to the maneuver state in Figure 6, Figures 14-15 illustrate the quality of the navigation parameters calculated based on the modified filter in comparison to the reference filter results in Figures 10 and 12.

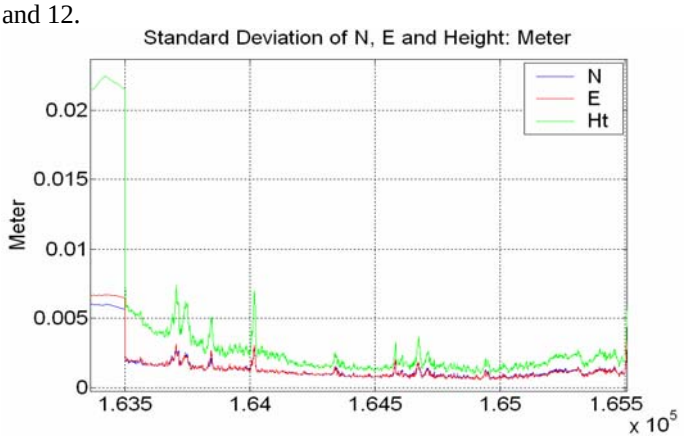

Figure 14: The STD of position in modified filter

As can be observed, the extended measurement filter improves the estimated standard deviation of the navigation parameters, which is still correlated, but much less than in Figure 10, to the platform maneuvers. The STD in position has mostly improved in the vertical channel, and particularly over shorter time periods as compared to the reference filter. Note that even in high dynamic situations, the STD in velocity has improved as expected, because the velocity information is fed directly to the filter.

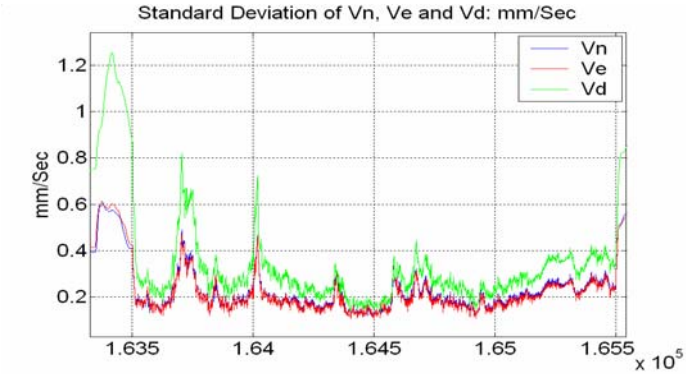

Figure 15: The STD of velocity in modified filter

6. CONCLUSION AND REMARKS

It was demonstrated that the GPS velocity observation, which is independent of the ambiguity terms, could improve the availability and continuity of the navigation solution in a tightly coupled integrated system. It should be mentioned that the cycle slip detection procedure is still necessary to avoid errors in the navigation solutions.

The test analysis of the impact of the velocity-updated filter on the overall quality of the navigation parameters indicates that steady navigation accuracy can be maintained even for extended time periods. The accuracy with respect to the reference solution was found to be within 14 cm for position, 3 mm/s for velocity and 20 arcsec for heading in our tests. In a steady portion, the difference is smaller than 5 cm for position, 2 mm/s for velocity and 10 arcsec for heading, respectively, which indicates that the velocity can provide quality solution. The precision of the navigation parameters in the steady state of trajectory is close to that of the reference solutions. Nevertheless, there is still need for other reference information, such as using imaging information with control points to independently assess the accuracy.

The velocity information, combined with the DD carrier phase, has improved the filter's sensitivity to the platform maneuvers. The RMS of fit in the navigation parameters provided by the extended measurement filter, which is designed based on the position and velocity information, has delivered the expected results. The accuracy with respect to the reference solution is within 5 cm for position, 2 mm/s for velocity and 10 arcsec for heading

The GPS velocity can be also used in land-based system. Land based mobile mapping systems often operate in urban environments where frequent losses of GPS lock may occur, and the time needed to fix the new ambiguity is excessive and preventing the filter from using any GPS information. Further study on applying this method in the land-based data reduction is planned. Moreover, the static alignment of INS system, the GPS velocity information can be also used to align the INS sensor in the dynamic mode.

ACKNOWLEDGEMENTS

The authors would like to thank Mr.Yudan Yi, the PhD student in the Department Civil and Environmental Engineering and Geodetic Science, OSU, for his help and assistance in the data reduction process.

REFERENCE

1. G. Siouris (1993); *Aerospace Avionics Systems A modern Synthesis*; Academic Press, pp: 269-373.

2. Gautier, J.D, B.W. Parkinson (2003), Using the GPS/INS Generalized Evaluation Tool (Comparison of Loosely coupled, tightly coupled and ultra-tightly coupled integrated navigation), Proc. ION Annual Meeting, June 24-25, pp. 65-76.
3. D.A.G. Brzezinska, R. Da, C. Toth (1998), GPS Error Modeling and OTF Ambiguity Resolution for High-Accuracy GPS/INS Integrated System, *Journal of Geodesy*, 72(11), pp. 628-638
4. B. Hofmann-Wellenhof, H. Lichtenegger, J. Collins (1994), *GPS Theory and Practice*, Springer-Verlag, pp: 186-191.
5. C. Jekeli, R. Garcia (1997), GPS phase acceleration for moving-base vector gravimetry, *Journal of Geodesy*, 71(10), pp. 630-639.
6. M.Szarmens, S. Ryan, G. Lachapelle (1997), DGPS High Accuracy Aircraft Velocity Determination Using Doppler Measurements, KIS97, Department of Geomatics Engineering, The University of Calgary, Banff(June)
7. J. Hebert, J. Keith, S. Ryan, M. Szannes, G. Lachapelle and M.E. Cannon (1997), DGPS Kinematic Phase Signal Simulation Analysis for Precise Aircraft Velocity Determination, ION Annual meeting, Albuquerque, NM, 3 June-2 July
8. C. Jekeli, (2001), *Inertial Navigation Systems with Geodetic Applications*, Walter de Gruyter, pp. 139-162.
9. Grejner-Brzezinska, D. A., Yi, Y., and C.K. Toth, (2001), Bridging GPS Gaps in Urban Canyons: Can ZUPT Really Help?, ION GPS 2001, Salt Lake City, September 12-14, CD-ROM.
10. Bar- Itzhack, IY, Berman, N (1988); Control theoretic approach to inertial navigation systems. *AIAA J Guidance, Contr. and Dynam.,* 11(3), pp. 237-245.
11. A. Gelb (1974), *Applied Optimal Estimation*, M.I.T PRESS, pp. 67-78.
12. D. Kim, R.B. Langley (2002), Instantaneous Read-Time Cycle-Slip Correction for Quality Control of GPS Carrier-Phase Measurements, *Journal Of the Institute of Navigation*, Vol.49, No.4, pp. 205-222